Tailor: understanding 3D shapes using curvature Ima-Cnr Technical Report n. 9 / 2001

Abstract

Tools for the automatic decomposition of a surface into shape features will facilitate the editing, matching, texturing, morphing, compression, and simplification of 3D shapes. Different features, such as flats, limbs, tips, pits, and various blending shapes that transition between them may be characterized in terms of local curvature and other differential properties of the surface or in terms of a global skeletal organization of the volume it encloses. Unfortunately, both solutions are extremely sensitive to small perturbations in the surface smoothness and to quantization effects when they operate on triangulated surfaces. Thus, we propose a multi-resolution approach, which not only estimates the curvature of a vertex over neighborhoods of variable size, but also takes into account the topology of the surface in that neighborhood. Our approach is based on blowing a spherical bubble at each vertex and studying how the intersection of that bubble with the surface evolves. For example, for a thin limb, that intersection will start simply connected and will rapidly split into two components. For a point on the tip of a limb, that intersection will usually simply remain connected, but the ratio of its length to the radius of the bubble will be decreasing. For a point on a blend, that ratio will exceed 2π. We describe an efficient approach for computing these characteristics for a sampled set of bubble radii and for using them to identify features, based on easily formulated f i lters, that may capture the needs of a particular application.

Categories and Subject Descriptors (according to ACM CCS): multiscale analysis, shape feature extraction, triangle-mesh decomposition.

1. Introduction

Shape analysis and coding are challenging problems in Computer Vision and Graphics. An ideal shape description should be able to capture and compute the main features of a given shape and organize them into an abstract representation which can be used to automate processes such as matching, retrieval or comparison of shapes. We have tackled the problem in the context of 3D objects represented by triangular meshes, having in mind that a good shape description should be able to distinguish between global and local features and should be based on geometric properties of the shape which are invariant under rotation, translation and scaling [6]. To characterize a shape we have used the paradigm of *blowing bubbles*: a set of spheres of increasing radius R_i, $i = 1,\ldots,n$ is drawn, whose centers are at each vertex of the mesh, and whose radius represents the scale at which the shape is analyzed. The number of intersections between the spheres and the shape boundary gives a first qualitative characterization of the shape in a 3D neighborhood of each vertex. Then, a number of metric and geometric parameters are computed to refine the classification and detect specific features such as sharp protrusions or wells, mounts or dips, blends or branching parts. An example of the resulting decomposition is given in Figure 1.

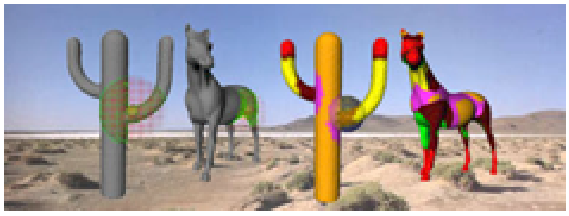

Figure 1: *Shape decomposition using blowing bubbles.*

The achieved description therefore provides an insight on the presence of features together with their morphological type, persistence at scale variation, amplitude and/or size.

The decomposition is algorithmically simple, independent on the orientation of the object in space and equally distributed in all directions. The multi-scale approach and the chosen descriptors define a view-independent decomposition and reduce the influence of noise on the shape evaluation. In this paper we focus on the method adopted for the segmentation, while a possible application of the results can be found in [13], where a skeleton describing a shape from the point of view of its sharpest protrusions is presented.

The paper is organized as follows: in Section 2 previous work relevant for the described method is briefly reviewed. Then, basic concepts on differential geometry delineate, in Section 3, the theoretical background of the used geometric descriptors. The approach to shape decomposition and several results are presented in Section 4. Future work and applications are described in the last Section.

2. Previous Work

Computing the description of a shape usually consists of the definition of a set of primitives, representing the features relevant to the specific context, and the construction of an abstract representation which encodes the computed description. In other words, the abstract model represents the shape structure with respect to the chosen basic shape primitives, whose geometric properties are measured by a set of descriptors.

As suggested in [12], methods for shape description can be classified into two broad categories: those considering only the boundary of the shape, and those measuring properties of the enclosed figure or volume. Typically, boundary-based methods are based on accurate and well-founded primitives, such as critical points or curvature extrema, but they generally lack in providing a global view of the shape, and do not significantly organize features into a hierarchy of global and local details.

Conversely, interior-based methods generally provide descriptions which better highlight the global structure of the shape. A traditional example are skeletons, such as the medial axis or the Reeb graph [1, 16]. The great advantage of skeletons is that they provide an abstract representation by idealized lines that retain the connectivity of the original shape, thus reducing the complexity of the representation. Usually, each arc identifies a portion of the original shape belonging to the same feature. For example, the medial axis is constructed using the paradigm of the maximal enclosed disks, whose centers define a locus of points which describes, together with the associated radius, the width variation of the shape. The medial axis induces a decomposition of the shape into protrusion-like features, while concavities of the shape are not directly identified by the medial axis. Unfortunately, the medial axis of a 3D shape is not any longer a one-dimensional graph, but it is made of surface pieces as well. Moreover, the instability of the medial axis with respect to noise has prevented its use in many application areas. Approaches to construct and store the medial axis at different scales have been also proposed, which implicitly address the problem of noise reduction as well [16, 3, 15].

Another notable example of topology-driven skeleton is given by the Reeb graph [18, 1]. The Reeb graph is a topological structure which codes a given shape by storing the evolution of criticalities of a mapping function defined on the boundary surface. In particular, when the height function is chosen with respect to a predefined direction, the Reeb graph describes the evolution of the contours obtained intersecting the shape with planes having the required orientation. The decomposition induced by the Reeb graph corresponds to a segmentation into shape parts where the topology does not change. The description obtained using a Reeb graph approach are suitable for matching purposes once the mapping function provides invariance under affine transformations [10, 13], at the cost of a less intuitive decomposition of the shape boundary. We propose here an alternative over this approach where we offer more flexibility to formulate the filters for shape analysis, and where a more inherent multi-resolution property is embedded in the characterization method.

3. Theoretical background

This section provides definitions and concepts [4, 8, 11, 14] useful for the description of our approach.

Let $x : D \subseteq \mathbf{R}^2 \mapsto \mathbf{R}^3$ be a C^2-parameterization of the surface

$$\Sigma := \{x(u,v) : (u,v) \in D\}.$$

The classification of local properties of Σ is traditionally based on the study of the *mean* and the *Gaussian* curvature, which can be respectively defined as the average and the product of the maximum and minimum principal curvatures [11].

Let us consider the normal n to the surface Σ at a point p, Let us now consider the *normal sections* of the surface around the normal vector, that is, the set of curves originated by intersecting the surface with planes containing the normal n. For each of these planar curves the curvature is classically defined as the inverse of curvature radius, and if we call k_1 the maximum of curvature of the normal sections, and k_2 the minimum, then we have that the mean curvature $\overline{\kappa}$ is defined as $\overline{\kappa} := (\kappa_1 + \kappa_2)/2$ and the Gaussian curvature as $K := \kappa_1\kappa_2$. The directions along which the extrema of curvature are assumed are called principal directions. This definition formalizes the relation between the surface shape and its position with respect to tangent plane. For example, for elliptic-shaped surfaces, the centers of curvature of all the normal sections will lie on the same side of the tangent plane, with positive values for the minimum and maximum of curvature. For hyperbolic-shaped surfaces, the centers of

curvature will move from one side of the surface to the other, with a negative minimum value and a positive maximum value assumed at opposite sides with respect to the surface. Finally, for parabolic-shaped surfaces, one of the principal directions will have curvature equal to zero, that is, along that direction the normal section will be a straight line. This is the case, in general, of ruled surface which are also said to have no double curvature. The planar case is obvious.

The Gaussian curvature represents a measurement at any point p of Σ which is the excess per unit area of a small patch of the surface, i.e., how *curved* it is. In spite of using a planar area (i.e. the tangent plane to Σ in p) to approximate a small patch on an arbitrary surface around p, it can be used a piece of sphere to achieve a better accuracy. An interesting result related to the Gaussian curvature is due to the Gauss-Bonnet theorem, which is introduced as follows.

First of all, given a closed curve γ on a surface Σ, let T_γ be the total turning that the unit tangent t undergoes when it is carried along γ, defined as the sum of the local turnings, i.e. *exterior angles* [11] (see Figure 2). Then, the quantity $I_\gamma = 2\pi - T_\gamma$ is called the *angle excess* of the curve γ and it is related to the curvature of Σ within γ, as described by the Gauss-Bonnet formula.

Gauss-Bonnet Formula
Let γ be a curvilinear polygon of class C^2 on a surface patch of class C^k, $k \geq 3$. Suppose γ has a positive orientation and its interior on the patch is simply connected. Then

$$\int_\gamma \kappa_g ds + \iint_\Omega K dS = 2\pi - \sum_i \alpha_i = I_\gamma \qquad (1)$$

where κ_g is the geodesic curvature along γ, Ω is the union of γ and its interior, K is the Gaussian curvature and α_i the exterior angles of γ.

Among the properties of the angle excess the following ones have a particular interest for our approach:

- I_γ is independent of the chosen starting point on γ,
- I_γ is additive,
- for any topological disk on an arbitrary surface around p, the angle excess around the boundary is equal to the total curvature of the interior.

Starting from the Gauss-Bonnet formula and defining the total curvature of Σ as the integral:

$$T_\Sigma := \iint_\Sigma K dS \qquad (2)$$

it can be proved that the last one is a topological invariant of compact, orientable surfaces as described by the following theorem.

Gauss-Bonnet Theorem

If Σ is an orientable, compact surface of class C^3, then

$$\iint_\Sigma K dS = 2\pi\chi(\Sigma) \qquad (3)$$

where $\chi(\Sigma)$ is the Euler characteristic of Σ.

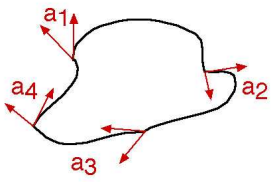

Figure 2: *Exterior angles $\{a_i\}$ on a closed path γ.*

The definition of the curvature at each point of a triangulation is not trivial because a triangular mesh is parameterized by a piecewise continuous function whose second derivatives are, almost everywhere, null. More precisely, the curvature on a triangulation is concentrated along edges and at vertices, since every other point has a neighborhood homeomorphic to a planar Euclidean domain whose Gaussian curvature is null.

The methods proposed in the literature for curvature evaluation can be classified in different ways but, as underlined in [7, 20], a global comparison among them still lacks. These methods can be divided into two main groups: *continuous-based* and *property-based* algorithms.

The first ones are developed transforming the discrete case to the continuous one by using a local fitting of the surface which enables to apply standard definitions. For example in [9] an approximation is derived at each vertex by applying the continuous definition to a least-square paraboloid fitting its neighboring vertices, while in [19] it is evaluated by estimating its tensor curvature. The second class of algorithms defines equivalent descriptors starting from basic properties of continuous operators but directly applied to the discrete settings. The methods proposed in [2, 17] are based on the Laplace-Beltrami operator, the Gauss map and the Gauss-Bonnet theorem guaranteeing the validity of differential properties such as area minimization and mean curvature flow [8].

In spite of the introduction of a multi-resolution structure, the mentioned approaches are usually sensitive to noise and small undulations, requiring smoothness conditions on the input mesh. Furthermore, the smoothing process used to get stable and uniform curvature estimations introduces a deficiency in the magnitude evaluation and, consequently, difficulties in the accurate distinction between planar patches and curved surfaces with low curvature.

Our framework is based on the use of the angle excess,

computed in the discrete domain represented by the triangular mesh. As presented also in [5, 17], the angle excess nicely evaluates the Gaussian curvature at mesh vertices. Let us consider the region $Star(p)$ on the surface de£ned by the triangles incident in a vertex p. The boundary of $Star(p)$ de£nes a closed path on the mesh, to which we may apply the Gauss-Bonnet formula (1). Since the geodesic curvature along the boundary is obviously zero (edges are straight), the total curvature at p is simply quanti£ed by the sum of the exterior angles. To understand better the geometry of the situation, we can imagine to locally cut $Star(p)$ along any of the edges incident in p, and to develop the $Star(p)$ onto the plane without shrinking the surface. The sum of the exterior angles corresponds to the sum of the angles at p in the $Star(p)$. This result is consistent with the intrinsic nature of the Gaussian curvature since the angle excess only depends on the angles, that is, this value does not change if the mesh is deformed preserving the distance between points. Also, the computation of the angle excess can be performed without resorting to any coordinate system, as the angles may be obtained using only the edge length and not the vertex coordinates.

4. Decomposition of triangular meshes

The approach proposed here for describing a 3D shape integrates boundary and interior information of the shape. The link between closed paths and curvature has suggested to specialize its study to the family of closed paths built by intersecting the surface with spheres centered in each of its points. The study of the evolution of these curves and the geometric characterization of the mesh areas intersected by the spheres are the core of the proposed method. The topology of the intersection curves changes according to the object shape: in Figure 3(a), the highlighted sphere intersects the surface only at one curve, while in (b) the boundary of the intersection area splits into two connected components. This is likely to happen, for example, near handles and branches, or around deep pits. Therefore, the variation in the boundary suggests that the vertex is in the proximity of a feature, which becomes relevant at the scale, or radius, at which the change occurs.

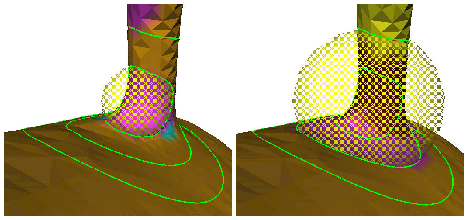

(a) (b)

Figure 3: *The evolution of intersection for increasing radii.*

Given a set of radii $R_i, i = 1, \ldots, n$, each vertex of the mesh will eventually be classi£ed with a n-dimensional vector of morphological labels, each corresponding to its type at the corresponding scale. Shape features of the mesh are then identi£ed by connected regions of vertices with the same label at a given scale, and the geometric parameters computed to assign the label will characterize the feature from a metric point of view. For example, a tip and a mount are both characterized by one intersection curve only, but they can be distinguished measuring the curvature induced by the intersection curve on the surface (see Figure 4).

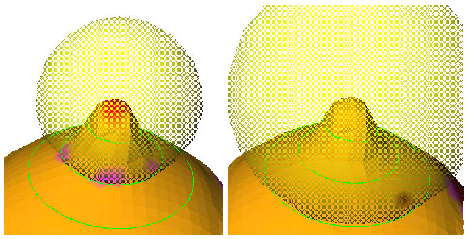

(a) (b)

Figure 4: *A tip measured for a small radius (a) becomes a mount at a larger radius (b).*

Features which are identi£ed by two intersection curves are further characterized by measuring the relative curve length and by checking if they define a volume which is inside or outside the shape (see Figure 5). These parameters, together with the persistence of type through the scale values, can be used to distinguish global and local features with respect to the scale range.

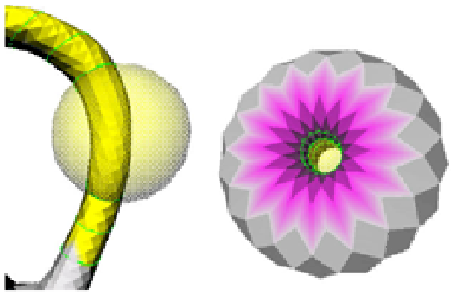

(a) (b)

Figure 5: *A handle (a) is distinguished by a narrow pit or through hole (b).*

As far as this paper is concerned, only the decomposition is fully described with less emphasis on the construction of the region adjacency graph which encodes the segmentation. In the following, the main steps of the procedure are detailed, starting from the computation of the intersections and from the f i rst basic classification according to the number of intersections. Then, the descriptors used to refine each class

are introduced. We distinguish between *geo-metric* descriptors, which are surface curvature and relative length of the intersection curves, and so-called *status* descriptors which distinguish between concave/convex or empty/full features. Finally, the segmentation will be summarized by presenting the complete characterization table, which defines the set of morphological labels used to decompose the surface. Results and discussions will conclude this section.

4.1. Computation of the intersections

Given a 3D mesh Σ and a set of radii $R_i, i = 1,\ldots,n$, let $S(p,R_i)$ be the sphere of radius R_i and center p, and $\gamma(p,R_i)$ the boundary of the region of Σ containing p delimited by the intersection curves between the mesh and $S(p,R_i)$. Other regions of intersection might occur, but only the one containing p is taken into account. The first morphological characterization of the surface at a vertex p at scale R_i is given by the number of connected components of $\gamma(p,R_i)$.

We consider the following cases:

- 1 *component*: the surface around p can be considered topologically equivalent to a plane (see Figure 6(a)),
- 2 *components*: the surface around p is tubular-shaped (see Figure 6(b)),
- $n \geq 3$ *components*: in a neighborhood of p a branching of the surface occurs (see Figure 6(c)).

In topological terms, two components identify a handle in the object, three or more components highlight a split. If $\gamma(p,R_i)$ is made by only one component, the angles excess is computed and the vertex is classified as sharp, smooth or blend. If $\gamma(p,R_i)$ is made by two components, their lengths are used to distinguish between conic and cylindrical shapes. For branching parts, no further geometric parameters are computed (see Table 1).

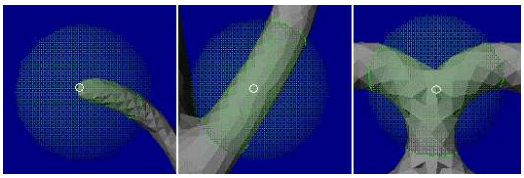

(a) (b) (c)

Figure 6: *Different number of connected components in the intersection boundary.*

To run the process, a set of radii must be selected for the computation of the intersections. The maximum and minimum radii (R_{max} and R_{min} respectively) determine an interval which is uniformly sampled according to the number of radii the user wants to use. This step produces the values of $R_i, i = 2,\ldots,n-1$ ($R_1 := R_{min}$ and $R_n := R_{max}$). Both R_{min} and R_{max} can be defined by the user by means of a slider in the GUI; otherwise, they are automatically set proportionally to the data set bounding box diagonal. It is desirable that R_{min} is at least equal to the minimum edge length of the mesh, otherwise we would face the problem of locality, as mentioned in Section 4.5.

The intersection between the sphere $S(p,R)$ centered in the vertex p of the triangulation and with radius R is achieved in the following steps (see Figure 7):

- starting from a triangle incident in p and moving toward γ a triangle intersected by $S(p,R)$ is selected,
- moving from the selected triangle and exploiting the adjacency relations the intersection curve is built.

This procedure ensures that only the boundary $\gamma(p,R)$ whose interior contains the vertex p is selected. We underline that the intersection between each triangle T and $S(p,R)$ is reduced to f i nd the roots of an equation of degree two where the unknown is used to parameterize the edges of T. As shown in Figure 7, the length of $\gamma(p,R)$, is given by the sum of the composing arc lengths, each one belonging to an intersecting triangle, and given by $R\theta$ where θ is the angle $\widehat{apb}$, a,b being the intersection points. The intersection curve is visualized using the associated 3D polygonal chain of intersection, defined by the edge-sphere intersections.

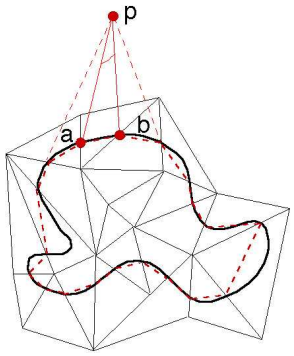

Figure 7: *Approximate length of the intersection paths.*

With reference to the properties of the obtained intersection curve $\gamma(p,R_i)$ at scale R_i, p is classified according to the number of connected components of $\gamma(p,R_i)$, curvature if $\gamma(p,R_i)$ has only one component, relative length if $\gamma(p,R_i)$ has two components, and a concavity/convexity check in all cases.

These classification criteria will be treated separately in the following sections. The combination of these classifications leads to a complete characterization of vertices, which expresses both the geometric and morphological properties of the surface.

4.2. Curvature characterization

As described in Section 3, when $\gamma(p,R)$ has only one boundary component, the curvature at a point p, at scale R, is approximated by the angle excess of $\gamma(p,R)$. Instead of using

the angle excess, we just use the length of $\gamma(p,R)$ divided by the radius R, i.e. $L_{\gamma(p,R)} = length(\gamma(p,R))/R$. Note that this value has the dimension of an angle and it always assumes a positive value. Since we want to characterize the curvature of a surface, vertices will be labelled as sharp, smooth, or blend points according to their approximated curvature values by establishing some thresholds on the interval $[0,+\infty)$. The choice of these thresholds does not represent a lack of generality, since they are tuned on the evaluated values on sample surfaces. We can distinguish the following cases:

- *sharp vertices*: let us consider a cone surface (see Figure 8), with p a spike point and $\alpha \in (0,\pi/2]$ the half amplitude of the cone. Intersecting the cone with a sphere centered in p and with radius R generates a circular curve of length $2\pi R\sin(\alpha)$ and a length value $L_\gamma(p,R) = 2\pi\sin(\alpha)$, which is an increasing function of $\alpha \in (0,\pi/2]$: the less is α, the more *pointy* is the surface around p. Intuitively, we consider p a sharp vertex if $\alpha \leq \pi/4$ and consequently the curvature threshold is set to $T_s = \sqrt{2}\pi$; anyway, the option of changing the threshold is available to the user who can tune the α value for each input surface.
- *smooth/blend*: to distinguish between these two situations we observe that the surface is smooth in a neighborhood of a point if its curvature continuously decreases, becomes at first f l a t and then *blend*. Now consider the intersection between the sphere and a plane; in this trivial case the length of the intersection curve is equal to $2\pi R$ and $L_\gamma(p,R) = 2\pi$; it follows that the threshold which discriminates between *smooth* and *blend* is set to $T_b = 2\pi$.

Summarizing, the characterization of a point p at scale R is set as follows:

- $0 \leq L_\gamma(p,R) \leq \sqrt{2}\pi$: p is *sharp*,
- $\sqrt{2}\pi < L_\gamma(p,R) \leq 2\pi$: p is *smooth*,
- $L_\gamma(p,R) > 2\pi$: p is *blend*.

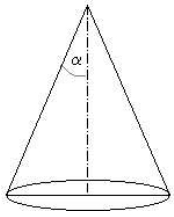

Figure 8: *Threshold shape for sharp features.*

4.3. Relative length characterization

Now consider the case of two connected components in the intersection curve $\gamma(p,R)$. As mentioned above, this means that p lies on a region of the surface having an elongated shape, like a tubular protrusion or a handle around a hole in the object. We can specialize this remark as follows: if the length of the two intersection components is nearly the same, the shape at scale R can be approximately considered cylindrical; if one is much longer than the other, it means that the shape may be seen as a conic part (see Figure 9). Let γ_1 and γ_2 be the two intersection components, and l_1, l_2 their lengths with $l_1 \geq l_2$. The shape is considered conical if $l_1 \geq 2l_2$. The related threshold is $T_c = 1/2$ thus guaranteeing that the amount l_2/l_1 (belonging to $[0,1]$) uniquely determines whether the local shape of the surface around p is cylindrical or conic.

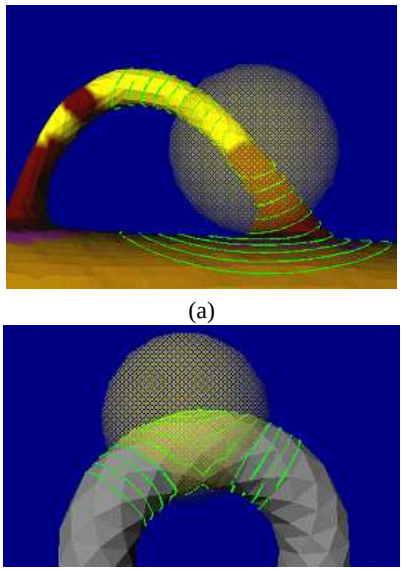

(a)

(b)

Figure 9: *Example of conical (a) and cylindrical (b) parts of a triangular mesh.*

4.4. Status characterization

The extraction of morphological features on a surface is based on different operators each of them provides a specific, e.g. geometric, topological, approach to its description. For instance in the case of one connected components in $\gamma(p,R)$, to discriminate between convex and concave vertices would lead to classify a *sharp* point as a peak or a pit, a *smooth* point as a mount or a dip. Obviously, the distinction between convex and concave does not make sense for blend points. An analogous to the convexity/concavity property is defined for vertices with two or more connected components in $\gamma(p,R)$. In this case, it is checked if the surface intersected by the sphere encloses a volume which is inside or outside the object. In other words, a criterion is used for distinguishing a handle from a deep tubular depression of the object.

Let us consider the case of one component f i rst. As for curvature computation, concavity/convexity evaluation at a vertex p of a triangular mesh is strongly affected by noise and it depends on the local topology of the $Star(p)$. The local

approach is depicted in Figure 10: a given edge e shared by triangles t_1, t_2 of a mesh is convex (resp. concave) if the angle formed by t_1, t_2, inside the object, is less (resp. more) than π.

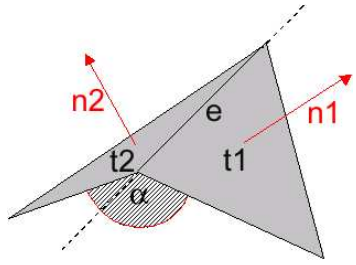

Figure 10: *Edge concavity or convexity criterion.*

Consequently, a given vertex p is defined strictly convex (resp. strictly concave) if all the incident edges in p are convex (concave). Because in most cases the incident edges in p are both convex and concave, the previous classification can not be applied. Furthermore, point coordinates can be slightly affected by noise resulting in a complete different classification. For these reasons, the method adopted for assigning a *convex* or *concave* label to a vertex p at scale R again uses the intersection between the mesh and the sphere. In the case of one connected component of the intersection curve, the center of mass b of γ and the average normal N of the intersected triangles are computed. The vertex p is considered concave (convex) at scale R, if p lies below (resp. above) γ, that is $N \bullet (b-p) > 0$ $(resp. < 0)$. We refer to Figure 11 for an easier understanding.

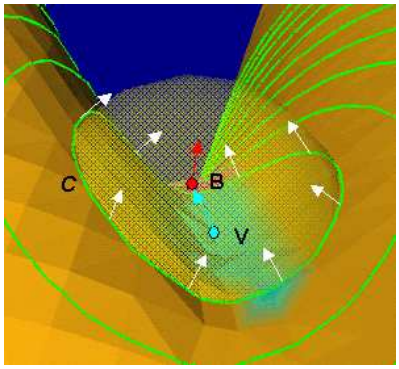

Figure 11: *Example of dip on a triangular mesh.*

Suppose now that $\gamma(p,R)$ has two intersection components. Again we can distinguish between the case in which the local shape is a tubular protrusion or a tubular well of the surface (see Figure 12), in analogy with the property of convex/concave mentioned above for points generating one intersection curve.

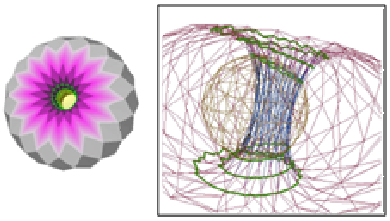

Figure 12: *Example of tubular through hole on a triangular mesh.*

If the connected components are two, we consider the orientation of each component of $\gamma(p,R)$ as naturally induced by the triangle orientation (see Figure 13(a)). It happens that if p lies on a tubular protrusion of the surface, the normal vector of the average plane related to each connected component of $\gamma(p,R)$ is directed towards p (see Figure 13(b)) according to the right-hand rule; if p appears on a tubular depression of the object, the vectors have opposite directions. This statement holds for three or more connected components too, thus it is possible to discriminate between a branch on the outer surface or a splitting cavity.

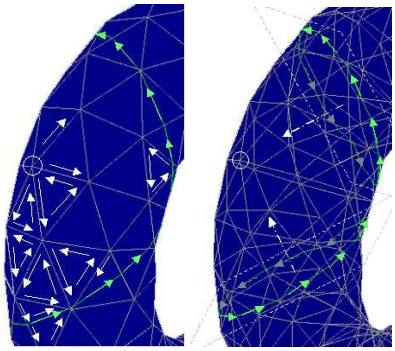

(a) (b)

Figure 13: *(a) Curve orientation derived by triangle orientation, (b) average normal of intersecting curves.*

4.5. Mesh decomposition

The focus of this section is the integration of the different characterizations to achieve a segmentation of the input mesh into morphological features represented by closed regions with uniform properties. In Table 1, a summary of the labels assigned to vertices for a given scale R is given.

The morphological classification associates a vector of feature labels to each vertex, and each label describes the vertex at the corresponding scale. Selecting the scale of interest, the surface can be rendered using a color-coding of the feature labels. The achieved decomposition is an

Table 1: *Morphological feature characterization.*

Feature	Color	#∩	Geo-metric	Status
TIP	red	1	$L/R \leq T_s$	convex
PIT	blue	1	$L/R \leq T_s$	concave
MOUNT	orange	1	$T_s < L/R \leq T_b$	convex
DIP	cyan	1	$T_s < L/R \leq T_b$	concave
BLEND	pink	1	$L/R > T_b$	–
LIMB	yellow	2	$L_2/L_1 \geq T_c$	full
WELL	violet	2	$L_2/L_1 \geq T_c$	empty
JOINT	brown	2	$L_2/L_1 < T_c$	full
FUNNEL	gray	2	$L_2/L_1 < T_c$	empty
SPLIT	green	≥ 3	–	full
HOLLOW-Y		≥ 3	–	empty

affine-invariant segmentation into disjoint, non-empty subsets which code the geometry and shape evolution through scale changes. In Figure 14 and 15 two examples are shown; the different views display the results obtained using a set of eight radii, and the colors are those related to Table 1. For each scale, a reference sphere is also drawn.

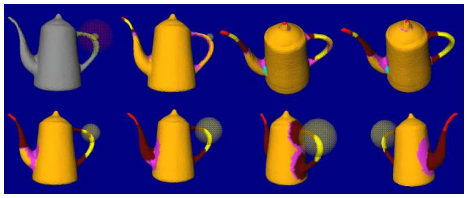

Figure 14: *Shape segmentation on the pot.*

4.6. Discussion on results

The defined tools allow us to analyze a shape at different scales, and to derive information about the persistence of a shape feature across the scale range.

It is interesting to notice the good behavior of the decomposition with respect to noise. In Figure 16, the decomposition of the original rabbit (a) and the rabbit with added noise (b) are shown, at the same scale of analysis. It can be seen that pointy features are still properly identified. As discussed in the previous sections, indeed, curvature-based segmentation algorithms usually involve local measures and therefore are affected by noise. With the proposed strategy, the curvature is analyzed in a neighborhood whose size depends on R: for small values of R, such as the average length of the edges incident in p, the curvature approximation resembles the discrete curvature estimation proposed in [2] and suffers of the same problems while, for increasing values, it becomes more stable to noise. On the other hand, a too large radius

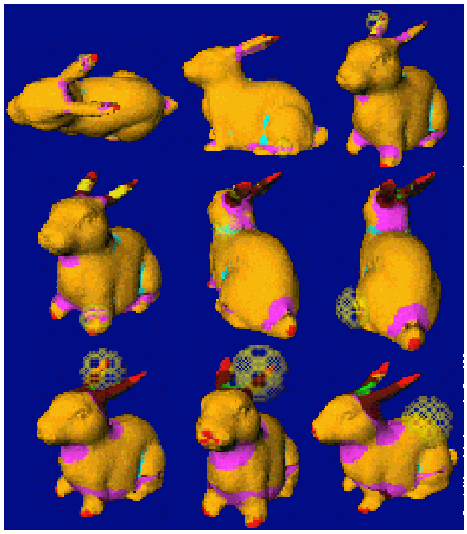

Figure 15: *Shape segmentation on the rabbit.*

can give a meaningless result. In the same way, small radii can be used to determine detail features while bigger ones are able to capture global characteristics of the surface. From these considerations, it follows that the choice of R is related to the scale of the features which have to be extracted, and the use of a set of increasing radii is suitable for performing a multiscale analysis of the shape.

(a) (b)

Figure 16: *Shape segmentation and noise.*

It is also possible to define a relational model induced by a set of queries each one represented by a specific relation and finalized at coding a particular level of representation of the object, as described in Table 1, thus providing a basic shape query language. The combination of these relations using logical operators enables the construction of a high-level language for shape interrogation guaranteeing a multitask model. In fact, the user is able to extract a single shape element only using a query, to combine them and, in future improvements, to locally change the geometry by us-

ing other surface patches or the topology by changing the structure of the surface graph.

Currently, a coarse feature-based query language is available, which allows the user to submit a query like "which are the vertices whose feature type is TIP at scale 3 and MOUNT at scale 6?", simply by means of a query vector with wild card, and the AND Boolean operator. For instance, the vector (*,*,P,*,*,M,*,*,*,*) would specify the above query. The results obtained (see Figure 17) suggest that further improvements of the query language will allow the extraction of higher-level features, like handles or main body of a given object. Tubular components can be extracted choosing LIMB OR JOINT vertices; among them, handles correspond to cycles in the region adjacency graph, and protrusions are adjacent to TIP or MOUNT zones. Selecting points which assumes TIP OR MOUNT OR DIP OR BLEND features at most levels of detail identify the main body of the object, and so on.

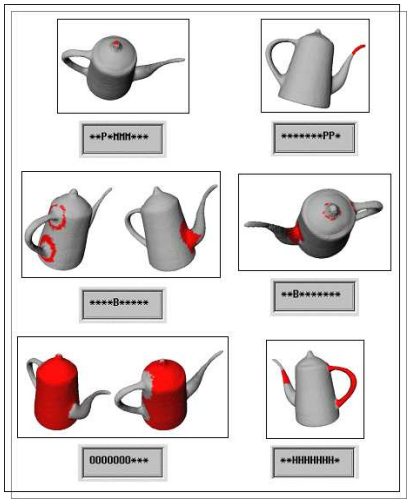

Figure 17: *Examples of queries on the pot.*

Using the described language, the mesh can be analyzed in a rather flexible way. Instead, if we are willing to extract a global shape classification which takes into account the whole range of scales into a single decomposition of the mesh, the following voting algorithm for persistence can be used. First, the points are classified according to the intersection connectivity, that is, according to the number of single, double or multiple components in the intersection boundary, considering the whole range of scales. The mesh is therefore segmented in parts which are characterized by having either almost always one intersections, or two or more. This step provides a first insight on features which are persistently protrusion-like, handle-like or branch-like, without distinguishing if they are convex/concave or full/empty. In Figure 18(a), the result of this segmentation is shown, where the blue parts are composed by vertices having only one intersection for more than the 75% of scales, the red are those having two intersections for the same threshold. Finally the grey areas are those corresponding to shape transitions where both one and two intersection approximatively occur in the same amount.

Within each of the resulting parts, a further classification can be done considering the related geometric characterization. For example, in Figure 18(b), the shape vertices are colored with different blue levels depending on the curvature; a deeper blue corresponds to a higher curvature. An analogous is applied to vertices with two intersection using their relative length where a lighter red is related to cylindrical-like features.

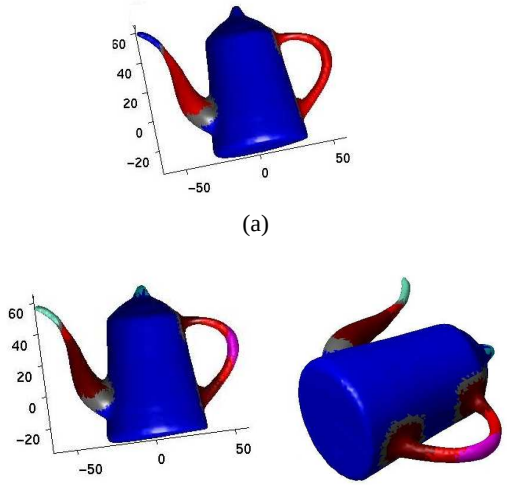

Figure 18: *Example of persistence analysis on the pot.*

5. Conclusions and future work

The evolution of intersection curves produced by blowing bubbles at mesh vertices has been proved to be a good approach to characterize the shape using meaningful shape features. Increasing the radius of the bubbles produces an easy and efficient multiscale analysis of the shape, which can be effectively used to produce a set of specific and flexible tools for shape analysis. The resulting description is an affine-invariant segmentation of disjoint, non-empty subsets and equally distributed in all directions, which codes the geometry and shape evolution through scale changes. Finally, the decomposition is algorithmically simple. The extracted information has a more general usefulness which is suitable not only for segmentation but also for the definition of a shape abstraction tool and of an editing model for triangular meshes. For example, can be used to find the seed points for the construction of an affine-invariant skeleton [13] which represents the input for a wide class of applications such as

matching and topological characterization of 3D-shapes (see Figure19).

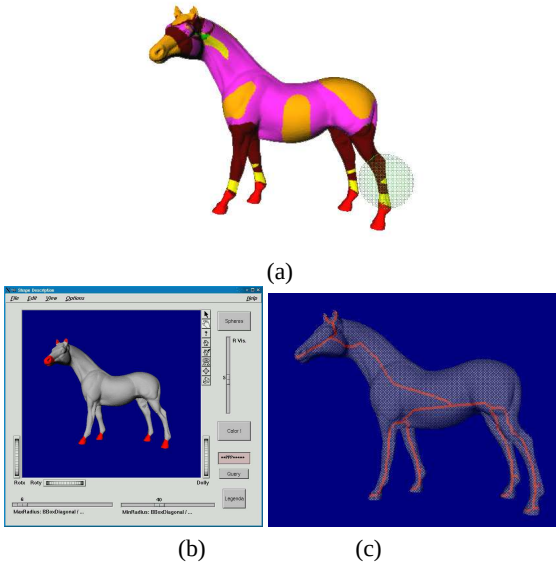

(a) (b) (c)

Figure 19: *(a) Segmentation on the horse, (b) example of query on the horse, (c) adjacency graph on the skeleton.*

Future developments will mainly focus on the definition of a feature adjacency graph and on the study of its evolution within the scale range required.

References

1. S. Biasotti, B. Falcidieno and M. Spagnuolo, "Extended Reeb Graphs for Surface Understanding and Description". *Proceedings of the 9th Discrete Geometry for Computer Imagery Conference, LNCS*, Springer Verlag, Uppsala, 2000. 2

2. M. Desbrun, M. Meyer, P. Schroeder, A.H. Barr, "Discrete Differential-Geometry Operators in *n*D", July 22, 2000. URL: http://www.multires.caltech.edu/pubs/pubs.htm 3, 8

3. Dill, A.R., Levine, M.D., Noble, P.B.: Multiple Resolution Skeletons. *IEEE Transactions on Pattern Analysis and Machine Intelligence*, Vol. PAMI-9, no. 4, 495-503,1987. 2

4. DoCarmo, M.: *Differential geometry of curves and surfaces*. New Jersey: Prentice Hall 1976. 2

5. Falcidieno, B., Spagnuolo, M.: Geometric Reasoning for the Extraction of Surface Shape Properties. *Communicating with the Virtual World*, N.Magnenat Thalmann and D. Thalmann (Eds.), Springer-Verlag, (1993) 3

6. Falcidieno, B., Spagnuolo, M.: A Shape-abstraction paradigm for modelling geometry and semantics. *Proceedings of Computer Graphics International 1998*, IEEE Computer Society Press (1998) 1

7. Gonzales, R.C., Woods, R.E.: *Digital Image Processing*. Reading, MASS.: Addison-Weshley, 1992. 3

8. V. Guillemin, and A. Pollack, *Differential Topology*, Englewood Cliffs, NJ: Prentice-Hall, 1974. 2, 3

9. B. Hamman: Curvature Approximation for Triangulated Surfaces, *Computing Suppl.* 8, 1993, pp. 139-153. 3

10. M. Hilaga, Y. Shinagawa, T. Kohmura, T.L. Kunii, "Topology Matching for Fully Automatic Similarity Estimation of 3D Shapes", in *Computer&Graphics, Proceeding of Siggraph 2001*, Los Angeles, 2001. 2

11. Lipschutz, M.M.: *Theory and Problems of Differential Geometry*. Schaum's Outline Series. 2, 3

12. Loncaric, S.: A survey of shape analysis techniques. *Pattern Recognition*, 31(8), 983-1001, 1998. 2

13. Mortara, M., Patané, G.: Affine-invariant skeleton of 3D-shapes. To appear in *IEEE Proceeding of International Conference on Shape Modelling and Applications 2002*, Alberta, Canada. 2, 9

14. Mortenson, M.E.: *Geometric Modeling*, John Wiley, 1985. 2

15. Ogniewicz, R.L.: Skeleton-space: a multiscale shape description combining region and boundary information. *Proceedings of Computer Vision and Pattern Recognition*, 746-751,1994 2

16. Pizer, S.M., Oliver, W.E., Bloomberg, S.H.: Hierarchical Shape Descripion Via the Multiresolution Symmetric Axis Transform. *IEEE Transactions on Pattern Analysis and Machine Intelligence*, Vol. PAMI-9, no. 4, 505-511,1987. 2

17. Polthier, K., Scmies, M.: Straighhtest Geodesic polhedral Surfaces. In H.C. Hege and K. Polthier, editors, *Mathematical Visualization*. Springer Verlag, 1998. 3

18. Y. Shinagawa, T.L. Kunii, and Y.L. Kergosien, "Surface Coding Based on Morse Theory", *IEEE Computer Graphics & Applications*, 1991, pp. 66-78. 2

19. Taubin, G., Estimating the Tensor Curvature of a Surface from a Polyhedral Approximation, *Fifth International Conference on Computer Vision (ICCV'95)*. 3

20. Trucco, E., Verri, A.: *Introductory to techniques for 3-D computer vision*. Prentice Hall, 1998. 3